Chemical Science

Accepted Manuscript

This article can be cited before page numbers have been issued, to do this please use: M. H. Gohari, P. Ghamari, E. Hamzehpoor, F. Effaty, T. Friši and D. Perepichka, *Chem. Sci.*, 2025, DOI: 10.1039/D5SC04390E.

ROYAL SOCIETY OF CHEMISTRY

rsc.li/chemical-science

View Article Online
DOI: 10.1039/D5SC04390E

Mechanochemical Synthesis of π-Conjugated Naphthotetrathiophene-Based Covalent Organic Frameworks and Their Post-modification via the Doebner Reaction

Mohammad Hossein Gohari[a], Pegah Ghamari[a,b], Ehsan Hamzehpoor[a], Farshid Effaty[a,c,d], Tomislav Friščić[a,d], Dmytro F. Perepichka[a]*

a. Department of Chemistry, McGill University,801 Sherbrooke St. W., Montreal, H3A 09B, Canada

b. Centre Énergie, Matériaux et Télécommunications, Institut National de la Recherche Scientifique, Varennes, Québec J3X 1S2, Canada

c. Department of Chemistry and Biochemistry, Concordia University, 7141 Sherbrooke St. West, Montreal, QC, H4B 1R6, Canada

d. School of Chemistry, University of Birmingham, Edgbaston, Birmingham, B15 2TT, United Kingdom

Abstract:

We report that mechanochemistry enables the synthesis of new π-conjugated covalent organic frameworks (COFs) based on naphthotetrathiophenetetracarbaldehydes 2TTN and 3TTN, expanding the scope of COF structures with two new isomeric tetradentate nodes. While recent studies have explored COF isomerism by varying bidentate linkers to tune electronic properties, the impact of *node* isomerism remains largely unexplored. Here, we overcome these limitations using mechanochemistry to access COFs based on insoluble fused polycyclic heteroaromatic monomers. These COFs exhibit broad absorption across the visible spectrum with 3TTN COFs showing a red-shifted absorption compared to their 2TTN-counterparts. Microwave-assisted post-modification of COFs via the Doebner reaction converts imine into quinoline linkages, enhancing the chemical stability of the COF. We explore the effect of the node structure (2TTN vs 3TTN), the network connectivity (phenylenediamine, biphenylenediamine and diquinoline) on optical band-gaps of the COFs. All COFs have shown a marked increase of electrical conductivity, by 6 orders of magnitude, upon p-doping with iodine. Quinoline-linked COF showed proton conductivity up to 1.2×10^{-3} S cm^{-1} at 60 °C and relative humidity of 75%. This work opens new directions for electronic modulation in COFs through *node* isomerism and offers a sustainable route to robust, tunable, heteroaromatic frameworks.

View Article Online
DOI: 10.1039/D5SC04390E

Introduction:

Covalent organic frameworks (COFs) are crystalline porous two-dimensional (2-D) or three-dimensional polymers with growing applications in materials science,[1-3] including chemical separation, proton conduction, sensing, and energy storage, due to their structural tunability.[1, 4, 5] Their predictable chemistry allows for precise tuning of optical properties.[6, 7] 2-D COFs with covalently linked subunits and π-stacking interlayers can support efficient charge transfer,[8] making them suitable for electronic device applications. Although the tunability of crystalline frameworks is fundamental motivation in COF research, the properties of these materials frequently emerge from serendipitous discoveries rather than rational design.[9-13] Studying the effect of isomerism in COFs has recently attracted attention as a mean to uncovering structure-property relationships in COFs without perturbing their symmetry and the overall topology of the framework. While a significant effort was focused on isomeric linkages,[6, 14-21] the influence of node isomerism on COF properties is almost unexplored.[22-24]

Thiophene stands as the most common building block in conjugated polymers and oligomers with many thousands of thiophene-based structures explored for their semiconducting properties.[25, 26] Incorporation of thiophene in COFs promise realization of nanoporous materials with high efficient charge transport and useful semiconducting, photocatalytic and related applications.[27-31] Nonetheless, among hundreds of different COFs developed over the last two decades, only a handful are based on thiophene nodes and linkers (**Scheme 1a,b, Supporting Table S6**).[1, 6, 28, 32-41] The wide development of thiophene based 2D-COFs is hindered by several challenges. one is the lower symmetry of thiophene linker (C_{2v}) compared to the commonly used phenylene (C_{2h}) which can introduce disorder in the framework.[38]

COFs with Lieb lattices are of particular interest as the unique band structure of such a lattice can result in unusual electronic and magnetic properties including ferromagnetism or superconductivity.[42, 43] Creation of such lattice requires tetrafunctional nodes but a few of such COF have been realized to date and in most cases their π-conjugation is limited by dihedral twist between the node and the linker.[44-46] In this regard, we reasoned that the planar isomeric naphthotetrathiophenes 2TTN and 3TTN nodes would be of significant interest for the synthesis of highly conjugated COFs (**Scheme 1**).

View Article Online
DOI: 10.1039/D5SC04390E

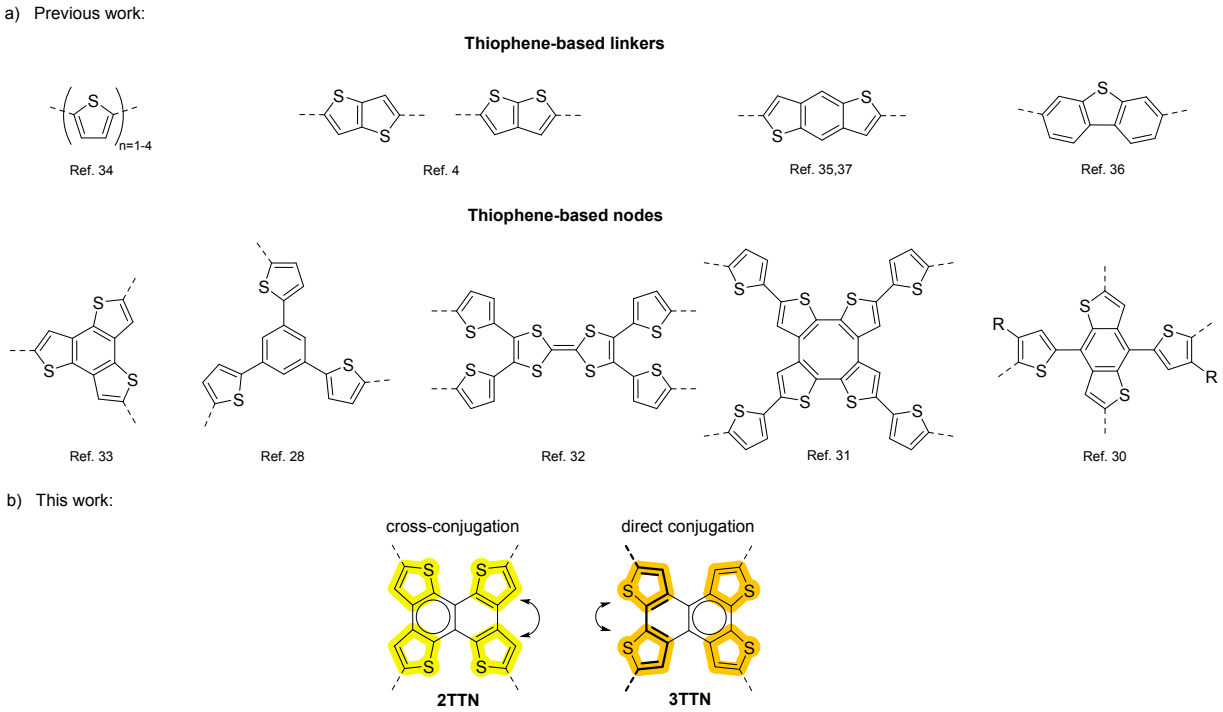

Scheme 1. a) Thiophene-containing linkers and nodes used in reported COFs. **b)** New isomeric naphthotetrathiophene (TTN) nodes reported here.

However, planarization and extension of polycyclic aromatic cores, such as in 2TTN and 3TTN, often result in poor solubility, which complicates the solvothermal COF synthesis. In principle, this challenge can be tackled by applying mechanochemical solvent-free methods which could also shorten the reaction time, lower the reaction temperature, and dramatically reduce the amount of generated waste, compared to the traditional solvothermal synthesis.[47] Since Banerjee et al. first introduced the mechanosynthesis of COFs via manual grinding,[48] this strategy has gained significant attention in the field.[49] Various mechanochemical techniques have subsequently been applied to the synthesis of COFs, including ball milling,[50, 51] screw extrusion,[52] and resonant acoustic mixing (RAM).[53] The majority of mechanochemically synthesized COFs are based on Schiff-base condensation reactions,[48, 50-52, 54-63] although other linkages such as boroxine[53] and triazine[64] have also been successfully explored using similar methodologies. Despite these significant advancements, only a small set of nodes have been used in mechanochemically synthesized COFs to date (**Table S7**).[48, 50, 53, 57-60, 64-66] A key challenge is that mechanochemically synthesized COFs typically exhibit low crystallinity compared to solvothermal products.[48, 51, 54-56, 64, 67] Furthermore, all of them rely on soluble precursors that can afford the same COFs (usually with superior crystallinity) via conventional solvothermal methods.

In this study, we introduce two isomeric tetrafunctional naphthotetrathiophene monomers, 2TTN-CHO and 3TTN-CHO, and use them in the mechanochemical synthesis of COFs with varied linkers (**Scheme 2**). We investigate how the connectivity of their thiophene units and the linker influence the photophysical properties of the resulting COFs and further investigate a Doebner reaction post-modification to transform imine-linked COF 2TTN-COF2 to quinoline-linked 2TTN-COF2-Q COF improving the chemical stability and shrinking the band gap by 0.4 eV.

View Article Online
DOI: 10.1039/D5SC04390E

2TTN-COF2-Q COF shows proton conductivity 3×10^{-4} S cm^{-1} at room temperature and relative humidity (RH) of ~75%.

Results and discussion:

Synthesis and characterization

To construct the target thiophene-based COFs, we have synthesized two isomeric tetrathienonaphthalene monomers, 2TTN-CHO and 3TTN-CHO. A lithiation-formylation sequence on the tetrathienylethylenes 2TTE and 3TTE (**Scheme 2, S1,S2**) affords the precursor aldehydes 2TTE-CHO[68] and 3TTE-CHO. Despite the strongly electron-withdrawing aldehyde groups, iodine-assisted photooxidative cyclization of 2TTE-CHO and 3TTE-CHO in the presence of methyloxyrane as an HI scavenger[69] resulted in 2TTN-CHO (91%) and 3TTN-CHO (50%), akin to those reported for unsubstituted 2TTE[70] and 3TTE.[71] The cyclized aldehydes precipitate from the reaction solution due to their low solubility (<10^{-4} M in DMF for 2TTN-CHO at room temperature) and were washed with organic solvents (DCM, methanol) and vacuum dried to afford pure solids (confirmed by ^{1}H NMR at 120 °C).

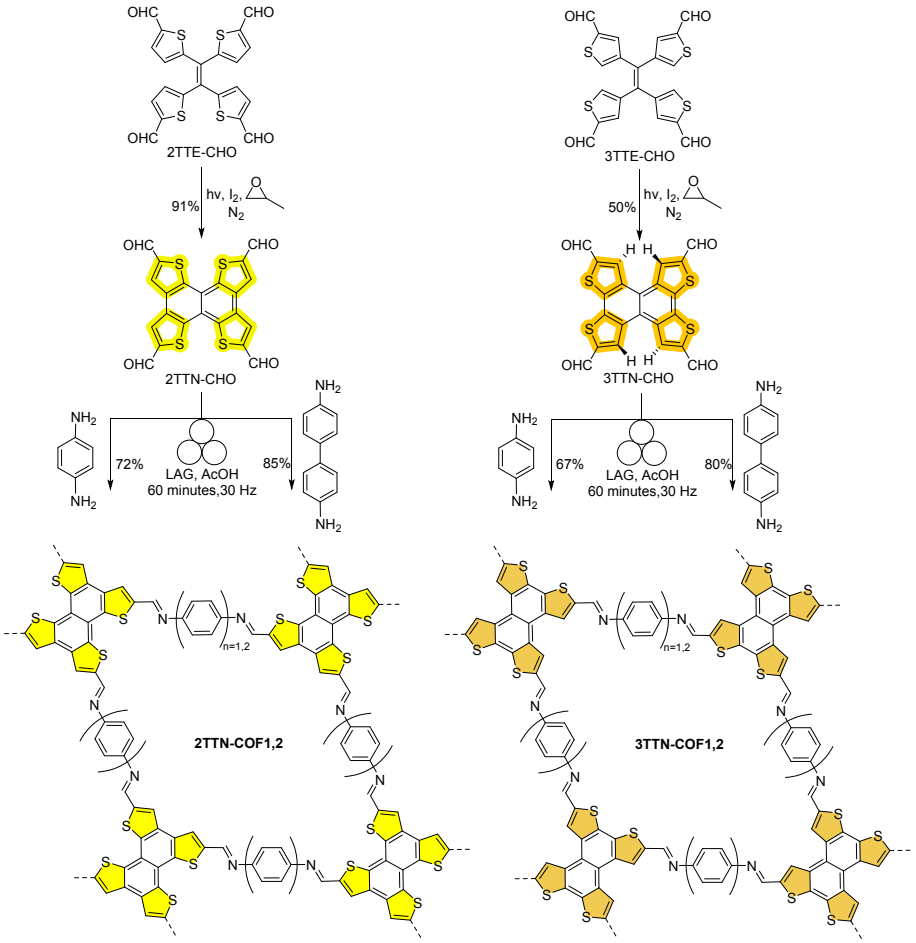

Scheme 2. Synthesis of TTN nodes and mechanochemical synthesis of naphthotetrathiophene-derived COFs.

View Article Online
DOI: 10.1039/D5SC04390E

Our initial attempts at solvothermal synthesis of 2TTN-COFs and 3TTN-COFs from the corresponding aldehydes with 1,4-diaminobenzene, resulted in poor conversions as evidenced by the remaining, highly insoluble, crystalline aldehyde monomers (**Figure S4a**). We thus turned to mechanochemical polymerization using a ball-milling method.

The reaction was optimized for the copolymerization of 2TTN-CHO with 1,4-diaminobenzene to construct **2TTN-COF1** in zirconia milling assembly (a 15 mL volume jar and a 2.6 g/10 mm diameter ball) (**Table S1a**). Using Lewis acid $Sc(OTf)_3$ as a catalyst with 1,4-dioxane as liquid additive only yielded the COF with low crystallinity. Changing the catalyst to acetic acid improved the crystallinity but residual diffraction peaks of the aldehyde could still be observed even at longer milling times (**Table S1a**, entry 4). Increasing the milling frequency from 25 to 30 Hz improved the crystallinity and conversion (**Table S1a**, entry 5). Increasing the amount of catalyst, liquid additive (the ratio of liquid additive to reaction mixture weight, η = 2.0-3.5 μL/mg) and replacing the liquid additive with THF had negligible effects on the crystallinity and the conversion in 60 minutes, which turned out to be the best (optimized) condition (**Table S1a,** entry 7). Lower ratio (η = 1.8), typically used in mechanochemical liquid-assisted grinding (LAG)[72] resulted in slightly higher crystallinity and conversion (**Table S1a**, entries 5, 9 and 2); however, these conditions proved less reproducible. The need for a higher amount of liquid could be attributed to trapping of the solvent in the pores of the forming COF.

Noteworthy, increasing the milling time from 60 minutes to 90 minutes significantly improved the conversion of aldehyde groups as screened by FTIR (**Table S1a**, entry 9; **Figure S18b**). However, the accessible surface area of the COFs is reduced from 493 m^2g^{-1} to 251 m^2g^{-1}, possibly due to pore collapse and/or pore blockade due to interlayer shift (**Figure S26g**).[53] Using softer milling materials, such as steel and Teflon, instead of zirconia resulted in incomplete COF formation as indicated by the presence of the aldehyde precursors in FTIR and PXRD (**Figure S6a, S18a, Table S1a entries 12-18**). The COF powders from the optimized condition were washed thoroughly with polar solvents (DCM, methanol, acetone), filtered under reduced pressure, and were further Soxhlet extracted to obtain pure, ambient air-stable, and highly crystalline powders.

Under the optimized reaction conditions, we also reacted 3TTN-CHO with 1,4-diaminobenzene, resulting in the formation of **3TTN-COF1** (**Table S1b**), as well as reacting both aldehyde precursors with benzidine, yielding **2TTN-COF2** and **3TTN-COF2**, respectively. To aid the structural characterization of COFs, model compounds were synthesized from 2TTN-CHO, 3TTN-CHO and aniline, under both solvothermal and mechanochemical methods.

The PXRD analysis of **2TTN-COF1** revealed a crystalline structure with Bragg reflections at 2θ = 5.0° and 9.9°, corresponding to the (100) and (200) planes (**Figure 1a**). A broad peak at 2θ ≈ 26° was attributed to the (001) plane, indicating weak long-range order along the *c* direction with interlayer spacing of ~3.4 Å. Pawley refinement suggests a monoclinic unit cell with *a* = 18.9 Å, *b* = 18.4 Å, *c* = 3.4 Å, α = β = 90.0°, γ = 97.9°. The PXRD analysis of **2TTN-COF2** showed Bragg reflections as 2θ = 4.1, and 8.1 (**Figure 1b, S3b**). For **3TTN-COF1**, the first reflection appeared at 2θ = 5.9 (100), and the unit cell was refined to *a* = 17.9 Å, *b* = 18.6 Å, *c* = 3.4 Å, α = β = 90.0°, γ = 65.8° (**Figure S3c**). PXRD of **3TTN-COF2** revealed peaks at 2θ = 4.8, and 8.7 (**Figure S3d**). The simulated diffraction patterns for the DFT-optimized unit cell closely matched the experimental data, reproducing both the reflection positions and the relative intensities suggesting an eclipsed (AA) interlayer orientation for all COFs (**Figure S3**).

View Article Online
DOI: 10.1039/D5SC04390E

The crystal structures of the unsubstituted 2TTN and 3TTN[71, 73] show that the former is completely planar while the latter exhibits a small twist of ~ 7° between out-of-plane hydrogen and naphthalene, brought about by steric repulsion between hydrogen in the bay area (**Scheme 2**). This out-of-place distortion may explain the slightly lower crystallinity of 3TTN COFs compared to 2TTN COFs. Scherrer analysis of the (100) reflection width suggests the crystal coherence length of ~ 14 nm for both **2TTN-COF1** and **2TTN-COF2** and lower values of ~ 9 nm for **3TTN-COF1** and ~ 13 nm for **3TTN-COF2**.

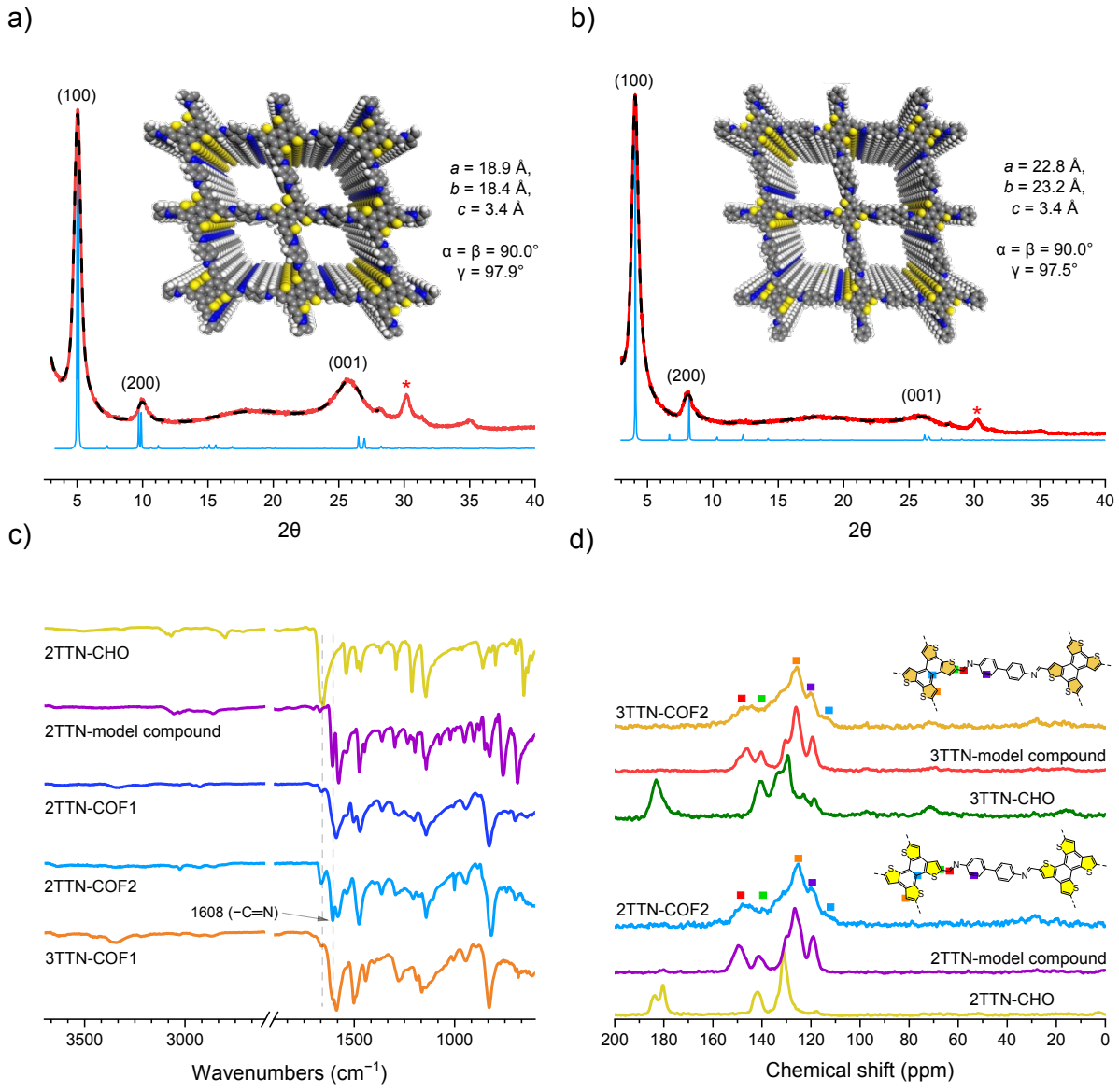

Figure 1. PXRD patterns of **a)** 2TTN-COF1 powder (observed (red), refined (dashed) and simulated AA stacking (blue), R_p = 2.15%, R_{wp} = 2.74%), **b)** 2TTN-COF2 (observed (red), refined (dashed) and simulated AA stacking (blue), R_p = 2.55%, R_{wp} = 3.45%), the inset shows the simulated structures. Full Width at Half Maximum (FWHM) is 0.57° and 0.56° for 2TTN-COF1 and -COF2, compared to 0.85° and 0.63° for 3TTN-COF1 and 3TTN-COF2 for 100 plane peaks, respectively (**Figure S3**). **c)** IR spectra of aldehydes,

View Article Online
DOI: 10.1039/D5SC04390E

model compound, and COF powders showing the imine linkages at 1608 cm^{-1}, residual aldehyde peak at 1660 cm^{-1}, and **d)** Comparison of ^{13}C NMR starting materials, model compounds and COF powders measured at (CP-MAS, 13 kHz). The peaks marked by * in a) and b) are due to trace amounts of zirconia leaching from jars (≤0.5% based on X-ray photoelectron spectroscopy (XPS), **Figures S6b, S9-S13**)

The IR spectrum of **2TTN-COF1** displays a characteristic C═N stretch at ~1608 cm^{-1} (**Figure 1c, Figure S17**). The dramatic decrease in the aldehyde C═O stretch indicates the reaction is nearly complete within 60 minutes of milling. Solid-state cross-polarization magic-angle-spinning (CP-MAS) ^{13}C NMR spectroscopy confirms the formation of the complete imine formation as indicated by the C=N peak at ~150 ppm and the disappearance of aldehyde groups at ~190 ppm (**Figure 1d, Figure S28**).

The elemental composition analysis obtained from the X-ray photoelectron spectroscopy (XPS) is in good agreement with the expected elemental composition for all 4 COFs (**Figure S9-S13**). For instance, for **2TTN-COF1**, the obtained elemental composition is 80.0 ± 0.5%, 9.1 ± 0.7%, and 7.4 ± 0.6% for C, N, S while the expected values are 81.0%, 9.5%, and 9.5%, respectively. The XPS also shows ~3.5% of oxygen present on the COF surface which we attribute to unreacted aldehyde groups, possibly chemisorbed water (as hemiaminal) and a small amount of ZrO_2 (0.13%) from the milling jar (**Figure S9, S10, Supporting section 12.2**).

Brunauer–Emmett–Teller (BET) analysis of the 77K nitrogen sorption measurements of vacuum-activated COFs (10^{-3} Torr, 120 °C, 24 h) suggest a relatively low surface area of 311 m^2/g for **2TTN-COF1** (theoretical 1584 m^2g^{-1}, **Figure S26a**). **2TTN-COF2** exhibits a higher surface area of 493 m^2g^{-1} (theoretical: 1793 m^2g^{-1}). However, both 3TTN COFs showed a much lower surface area of 23-90 m^2/g (**Figure S26**), which is in line with their lower crystallinity. We attribute this low surface area of all four COF to the interlayer slippage/pore collapse during the milling. [48] The pore size distribution obtained from the quenched-solid density functional theory (QS-DFT) of the N_2 isotherm data for **2TTN-COF1** corresponds closely to the micropore dimensions expected for the COF (19 Å) with contributions of mesopores at ~35–50 Å (**Figure S26h**).

The scanning electron microscopy (SEM) image shows micrometer-sized particles, with occasional plates reaching up to 100 μm for **2TTN-COF1** and **3TTN-COF1** (**Figure S27**). Thermogravimetric analysis (TGA) confirms that all COFs are stable up to at least 300 °C, with the highest stability observed for **2TTN-COF1** with T_{dec}^{95} ~440 °C (**Figure S20**).

Postmodification of COFs via Doebner reaction

Imine COFs exhibit limited hydrolytic stability and limited π-electron delocalization due to the polarity of the C=N linkage.[74] Various post-synthetic modification strategies have been developed to improve the stability and π-conjugation of imine COFs.[75, 76] These strategies often involve harsh conditions.[77] Notably, the Doebner reaction improves chemical stability and introduces functionality for various applications under mild reaction conditions.[78, 79] The combination of the electron-rich TTN node with the electron-withdrawing quinoline linkage is expected to lower the band gap compared to its imine-linked COFs.

View Article Online
DOI: 10.1039/D5SC04390E

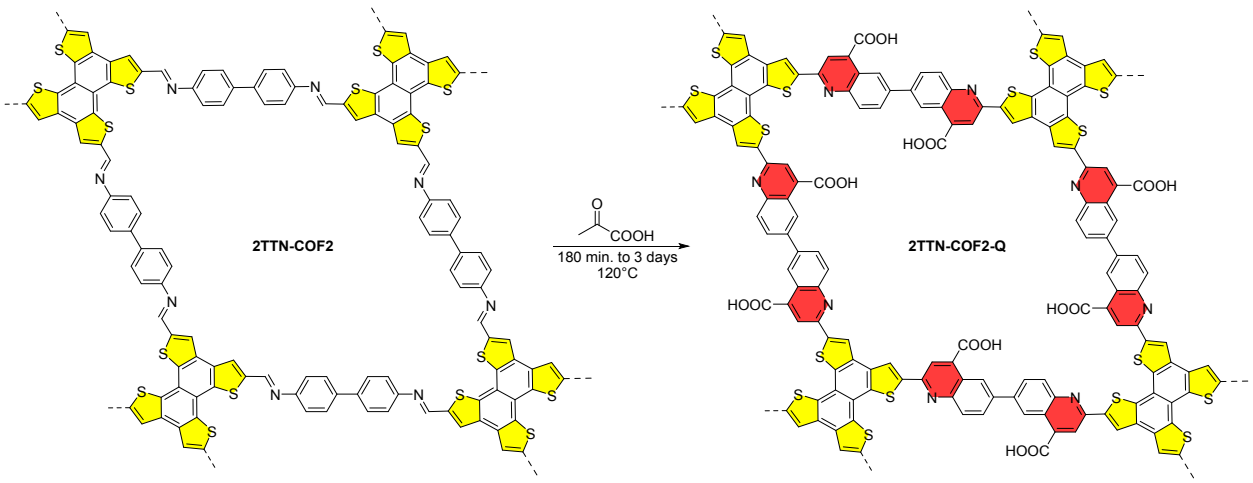

Scheme 2. Post-synthetic modification of 2TTN-COF2 for synthesis of quinoline-linked 2TTN-COF2-Q.

2TTN-COF2, which exhibits the highest crystallinity and largest pores in this series, was selected for post-modification. Using a modified Doebner reaction condition[78] (**Table S8**), the imine-linked **2TTN-COF2** was reacted with pyruvic acid in air atmosphere to obtain quinoline-linked **2TTN-COF2-Q** in 75% yield. The addition of small amounts of the free benzidine linker was essential to prevent the hydrolysis of imine bonds during the reaction, which otherwise leads to formation of the aldehyde monomer observed in the PXRD of the post-modified COF (**Figure S4b**).

Unlike imine-linked TTN COFs, which undergo complete dissolution in acid catalyzed aminolysis with hexylamine[80] (**Figure S2**), quinoline links are completely stable in these conditions. To assess the efficiency of the post-modification, the resulting **2TTN-COF2-Q** was reacted with hexylamine to digest the unconverted imine-linked domains. Such aminolysis of **2TTN-COF2-Q** prepared under solvothermal conditions resulted in 67% mass retention for **2TTN-COF2-Q**. The conversion yield can be increased by performing the Doebner reaction in solvent-free conditions (77% mass retained after aminolysis, **Supporting section 5**) but with a significant loss of crystallinity (**Figure S7**). On the other hand, this reaction can be accelerated (3 h, 120 ^{o} C) using microwave-assisted heating[81, 82] while maintaining the crystallinity (**Figure S7**) and achieving comparable conversion (57% mass retention after aminolysis).

The IR spectra of **2TTN-COF2-Q** COFs (**Figure 2b, Figure S19**) display characteristic peaks at 1704 cm^{-1} corresponding to the carboxylic group. The higher peak relative intensity of the carboxylic group in solvent-free approach compared to solvothermal and microwave-assisted, agrees with the higher conversion of the imine-linked COF in this approach (**Figure S19**). CP-MAS ^{13}C NMR spectrum shows the additional peak at ~170 ppm corresponding to the carboxylic group (**Figure 2c, Figure S29**). The XPS analysis of the 2TTN-COF2Qs shows an expected increase in the amount of oxygen (11.8%) and an overall good match of elemental composition with theoretical values (with deviations ≤1.3%, **Table S2**).

The surface area of **2TTN-COF2-Q** (solvothermal) is reduced to ~190 m^2g^{-1}, which is in agreement with the reduced pore size of the quinoline-linked COF (**Supporting section 12.8**). Thermogravimetric analysis (TGA) of post-modified COFs shows lower thermal stability

View Article Online
DOI: 10.1039/D5SC04390E

compared to imine-linked COFs (**Figure S20**). TGA-IR measurements of the Doebner post-modified COF confirm that the significant mass loss observed between 180 °C and 500 °C is attributed to CO_2 evolution from decarboxylation. The measured mass loss of 14.7% in this temperature range aligns well with the theoretical 17% mass loss calculated for the conversion of the 4-carboxyl-quinoline-linked COF to the quinoline-linked COF (**Figure S21**).

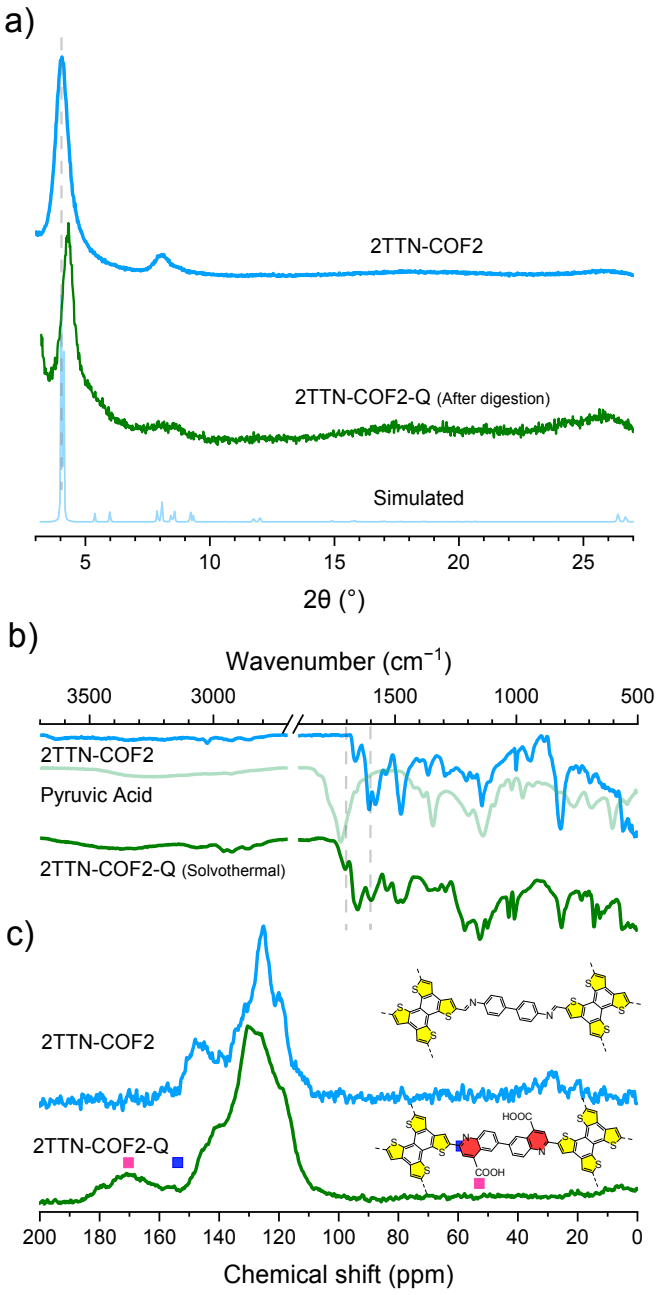

Figure 2. a) Experimental (blue) PXRD of 2TTN-COF2, experimental (green, background corrected), and simulated (light blue, AA stacking) PXRD of 2TTN-COF2Q synthesized solvothermally (after digestion). **b)** IR spectra of 2TTN-COF2Q, compared to 2TTN-COF2 and pyruvic acid. **c)** CP/MAS ^{13}C NMR spectra of 2TTN-COF2 and 2TTN-COF2-Q measured at 13 kHz.

View Article Online
DOI: 10.1039/D5SC04390E

Photophysical characterization

The optical properties of the COF powders were analyzed using diffuse reflectance spectroscopy (DRS), and their direct optical band gaps (E_g) were determined from Tauc plots (**Figure S22b**). The as-prepared TTN COFs exhibited broad absorption across the visible spectrum (**Figure 3a**, **Figure S22**). The absorption band of **3TTN-COF1** is red-shifted compared to 2**TTN-COF1** by 20 nm, which corresponds to a decrease in band gap from 1.89 eV to 1.81 eV. The effect is likely a result of the enhanced intra-sheet electron delocalization via 3TTN vs 2TTN core, which can be rationalized in the context of direct conjugation through the bithiophene moiety in 3TTN vs cross-conjugation in 2TTN (**Scheme 1c**). Indeed, DFT calculations (B3LYP/6-31G(d)) on 2-D COF monolayers reveal a narrower band gap for **3TTN-COF1** (2.78 eV) compared to **2TTN-COF1** (3.35 eV), despite the reduced planarity of **3TTN-COF1**. Furthermore, 3TTN-CHO also shows a redshifted emission compared to 2TTN-CHO in solution (**Figure S8d**). On the other hand, a blueshifted absorption of the biphenyl-linked **2TTN/3TTN-COF2** vs phenyl-linked **2TTN/3TTN-COF1** can be attributed to the twist in the biphenyl linker which limits the π-conjugation.[83, 84]

Converting the imine linker to a quinoline moiety results in a significant band gap contraction in the case of **2TTN-COF2-Q** (~1.7 eV, **Figure S22b**) which is in line with narrower calculated band gaps for this COF. This is consistent with enhanced π-conjugation and the formation of a donor-acceptor structure. While both the HOMO and LUMO in **2TTN-COF2** are primarily localized on the TTN core, the LUMO in quinoline-linked **2TTN-COF2-Q** is mainly located on the electron withdrawing linkage leading to more stabilization (0.1 eV) and reduced band gap (**Figure 3b, S14, Table S3**).

The ionization potentials (IPs) of the COFs were measured using Photoelectron Yield Spectroscopy in Air (PESA, **Figure 3c, Figure S16**). Phenyl-linked COFs showed slightly lower IPs (5.43 eV for **2TTN-COF1** and 5.46 eV for **3TTN-COF1**) than biphenyl linked COFs (5.55 eV for **2TTN-COF2** and 5.58 eV for **3TTN-COF2**). Converting the imine links in **2TTN-COF2** to quinoline leads to a ~0.1 eV decrease in IP for **2TTN-COF2-Q** (5.45 eV), consistent with its lower band gap. A summary of the energy levels of the COFs is presented in **Figure 3b** and **Table S3**.

View Article Online
DOI: 10.1039/D5SC04390E

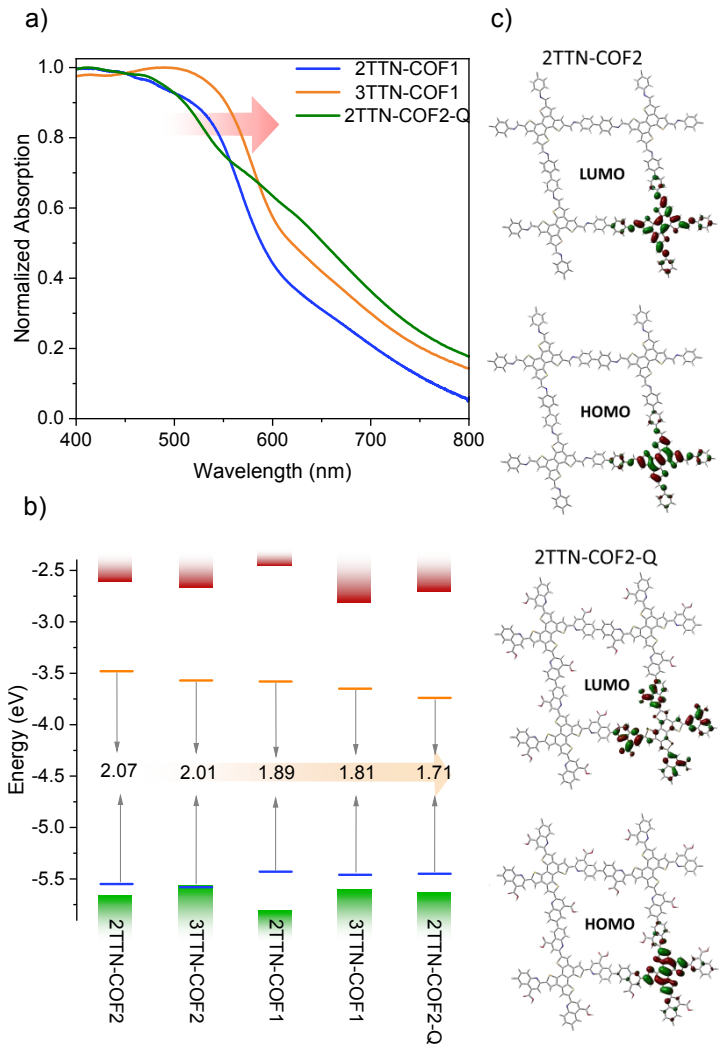

Figure 3. a) Diffuse reflectance spectrum of the COF powders. **b)** DFT-calculated (B3LYP/6-31G(d), red and green rectangles) and experimental (blue lines: PESA; orange lines: PESA + optical band gap) electronic levels of the COFs, and **c)** DFT calculated orbital topologies for 2TTN-COF2 (top) and 2TTN-COF2Q (bottom).

Electronic and proton conductivity

The *dc* electrical conductivity of TTN COFs was evaluated in compressed pellets using a two-probe measurement. Pristine COFs exhibited vanishingly low conductivities of 10^{-10}…10^{-11} S cm^{-1} (**Figure S30**). Doping in iodine vapor overnight improved the conductivity by up to six orders of magnitude (**Figure 4a**). Specifically, electrical conductivity of 3.2×10^{-4} S cm^{-1} and 1.7×10^{-5} S cm^{-1} was measured for phenylene-linked **2TTN-COF1** and **3TTN-COF1**, respectively. A lower conductivity was found in biphenylene-linked **2TTN-COF2** and **3TTN-COF2** (7.6×10^{-5} S cm^{-1} and 4.1×10^{-6} S cm^{-1}, respectively), while biquinoline-linked **2TTN-COF2-Q** showed slightly enhanced conductivity of 1.1×10^{-4} S cm^{-1} (**Figure S30**).

View Article Online
DOI: 10.1039/D5SC04390E

The absorption of iodine-doped COFs is red-shifted compared to pristine samples, with a low-intensity tail extending far in the near-IR region (**Figures 4c and S23**). The Electron Spin Resonance (ESR) spectroscopy shows an emergence of a strong signal upon doping, attributed to radical cations (**Figures 4b and S31**). However, the measured spin concentration is rather low (0.2-0.3% for **2TTN-COF1** and **2TTN-COF2** and 1% for **3TTN-COF1**). It is likely that the relatively high ionization potentials (**Figure 3c**) and possibly the instability of radical cation limit the generation of free carriers and thus the electrical conductivity of these COFs.

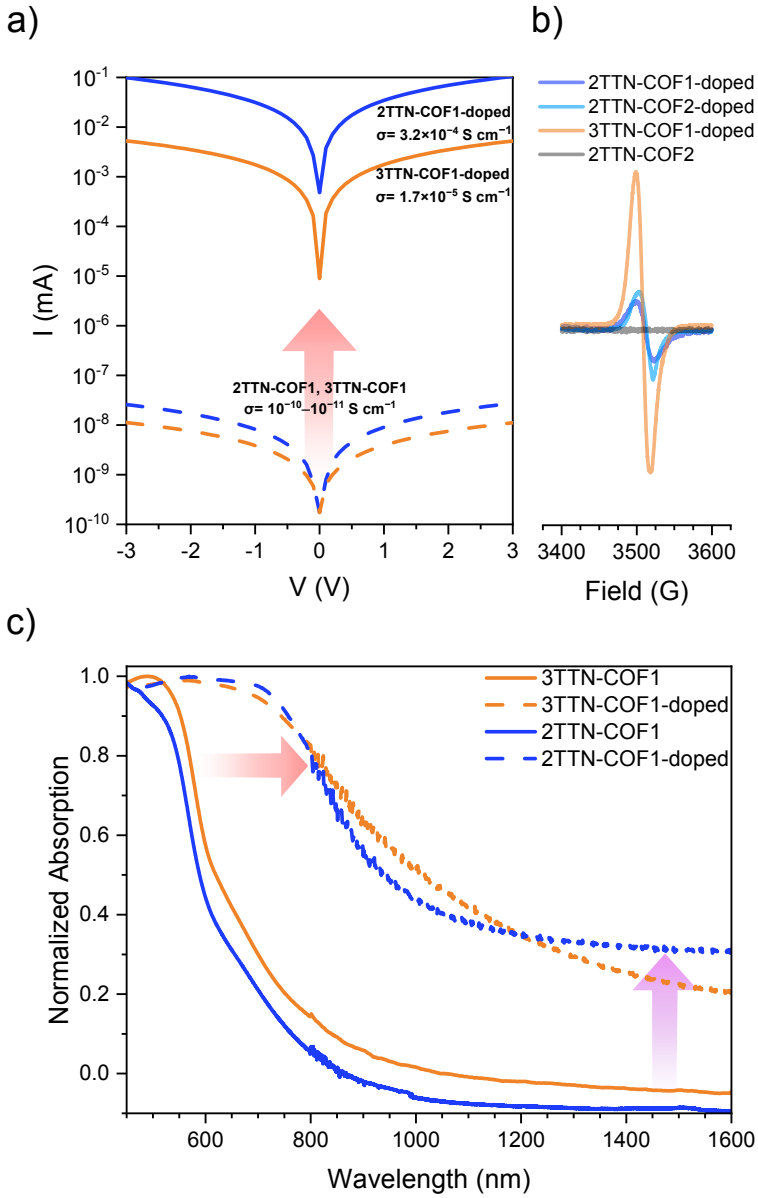

Figure 4. a) Comparison of log scale of electrical conductivity measurements of pristine and I_2-doped 2TTN-COF1 and 3TTN-COF1; **b)** EPR signal of pristine and I_2-doped COFs at room temperature in air; **c)** diffuse reflectance spectrum of the pristine and I_2-doped COF powders showing significant redshift upon doping.

View Article Online
DOI: 10.1039/D5SC04390E

Considering the growing interest in proton-conducting COFs,[85-87] we evaluated the proton conductivity of **2TTN-COF2-Q** using electrochemical impedance spectroscopy (EIS) on compressed pellets doped with H_3PO_4, under both non-hydrous (vacuum-dried samples) and humid conditions (equilibrated overnight at RH ~75%). Analysis of the Nyquist plots revealed a reasonably high room-temperature proton conductivities of ~1.4×10^{-4} S cm^{-1} in freeze-dried sample, but only a moderate increase to ~3×10^{-4} S cm^{-1} after humidification (**Figure S32**). A further increase of proton conductivity to 1.2×10^{-3} S cm^{-1} was observed at 60°C. These values are lower than 10^{-2} S cm^{-1} reported in a vinylene-linked triazine COF[87] under comparable conditions and the record ~10^{-1} S cm^{-1} reported for a ketoenamine-linked azo-COF at saturated humidity (RH ≈ 98%) at higher temperature.[88] We speculate that the basicity of the quinoline nitrogen may increase the binding of protons in the COF cavity and limit the conductivity.

Conclusion

In summary we have introduced two new isomeric tetragonal π-conjugated naphthotetrathiophene isomers as core for COF synthesis, and synthesized imine-linked COFs via mechanochemistry which was not readily accessible through typical solvothermal condition. The synthesized COFs show high crystallinity with permanent porosity and optical band gap ranging from 1.81 eV to 2.07 eV. We further post-modified 2TTN-COF2 using the Doebner reaction via solvothermal condition to yield quinoline linked 2TTN-COF2-Q reducing the band gap of the COF by about 0.4 eV with a slight improvement on the conductivity of the COF and a significant improvement of chemical stability. Both experimental and DFT results show that the structural differences in the TTN-COFs lead to different π-conjugation and planarity, which significantly impact their optical and electronic properties. We also developed microwave-assisted Doebner post-modification synthesis of quinoline-linked COF which significantly shortens the reaction time compared to the conventional solvothermal conditions. Due to the relatively high ionization potential (≳5.5 eV) of these COFs, only low charge carrier concentration (0.2-0.3%) can be introduced by doping with iodine. Nevertheless, such doping increases the electrical conductivity by 6 orders of magnitude (up to 3×10^{-4} S cm^{-1}) indicating pronounced charge transport properties of TTN-based COFs. Quinoline-linked COF showed proton conductivity of 1.2×10^{-3} S cm^{-1} at 60 °C and moderate RH (~75%). Our results showcase the advantages of mechanochemistry in providing straightforward access to COFs based on insoluble monomers, opening the opportunities for design of such materials based on large poly(hetero)cyclic building blocks with tailorable optoelectronic properties.

Conflicts of interest

There are no conflicts to declare.

Acknowledgements

This work was supported by NSERC of Canada. The authors thank Dr. Hatem M. Titi for his help with PXRD acquisition and useful discussions. The authors thank Dr. Alexander Wahba and Nadim Saade for the mass spectrometry analysis. The authors thank Dr. Kirill Levin for assistance with EPR measurements and VT NMR, Mr. Petr Fiurasek for support with DRS and IR spectroscopy. The authors appreciate useful discussions with Dr. Chang Wan Kang. M.H.G

View Article Online
DOI: 10.1039/D5SC04390E

acknowledges support from the FRQNT Doctoral Fellowship. The authors gratefully acknowledge Anaïs Hamelin (Audrey Moores' group) for assistance with the microwave reaction setup, and Jashanpreet Kaur (Janine Mauzeroll's group) for support with EIS measurements.

References:

1. K. Geng, T. He, R. Liu, S. Dalapati, K. T. Tan, Z. Li, S. Tao, Y. Gong, Q. Jiang and D. Jiang, Covalent Organic Frameworks: Design, Synthesis, and Functions, *Chem. Rev.*, 2020, **120**, 8814-8933.
2. A. P. Côté, A. I. Benin, N. W. Ockwig, M. O'Keeffe, A. J. Matzger and O. M. Yaghi, Porous, Crystalline, Covalent Organic Frameworks, *Science*, 2005, **310**, 1166-1170.
3. R. Liu, K. T. Tan, Y. Gong, Y. Chen, Z. Li, S. Xie, T. He, Z. Lu, H. Yang and D. Jiang, Covalent organic frameworks: an ideal platform for designing ordered materials and advanced applications, *Chem. Soc. Rev.*, 2021, **50**, 120-242.
4. Q. Gu, X. Lu, C. Chen, X. Wang, F. Kang, Y. Y. Li, Q. Xu, J. Lu, Y. Han, W. Qin and Q. Zhang, High-Performance Piezoelectric Two-Dimensional Covalent Organic Frameworks, *Angew. Chem. Int. Ed.*, 2024, **63**, e202409708.
5. Q. Gu, J. Zha, C. Chen, X. Wang, W. Yao, J. Liu, F. Kang, J. Yang, Y. Y. Li, D. Lei, Z. Tang, Y. Han, C. Tan and Q. Zhang, Constructing Chiral Covalent-Organic Frameworks for Circularly Polarized Light Detection, *Adv. Mater.*, 2024, **36**, 2306414.
6. R. Guntermann, L. Frey, A. Biewald, A. Hartschuh, T. Clark, T. Bein and D. D. Medina, Regioisomerism in Thienothiophene-Based Covalent Organic Frameworks─A Tool for Band-Gap Engineering, *J. Am. Chem. Soc.*, 2024, **146**, 15869-15878.
7. F. Kang, X. Wang, C. Chen, C.-S. Lee, Y. Han and Q. Zhang, Construction of Crystalline Nitrone-Linked Covalent Organic Frameworks Via Kröhnke Oxidation, *J. Am. Chem. Soc.*, 2023, **145**, 15465-15472.
8. M. Calik, F. Auras, L. M. Salonen, K. Bader, I. Grill, M. Handloser, D. D. Medina, M. Dogru, F. Löbermann, D. Trauner, A. Hartschuh and T. Bein, Extraction of Photogenerated Electrons and Holes from a Covalent Organic Framework Integrated Heterojunction, *J. Am. Chem. Soc.*, 2014, **136**, 17802-17807.
9. W. Zhao, P. Yan, B. Li, M. Bahri, L. Liu, X. Zhou, R. Clowes, N. D. Browning, Y. Wu, J. W. Ward and A. I. Cooper, Accelerated Synthesis and Discovery of Covalent Organic Framework Photocatalysts for Hydrogen Peroxide Production, *J. Am. Chem. Soc.*, 2022, **144**, 9902-9909.
10. F. Liu, P. Zhou, Y. Hou, H. Tan, Y. Liang, J. Liang, Q. Zhang, S. Guo, M. Tong and J. Ni, Covalent organic frameworks for direct photosynthesis of hydrogen peroxide from water, air and sunlight, *Nat. Commun.*, 2023, **14**, 4344.
11. Q. Huang, W. Li, Z. Mao, L. Qu, Y. Li, H. Zhang, T. Yu, Z. Yang, J. Zhao, Y. Zhang, M. P. Aldred and Z. Chi, An exceptionally flexible hydrogen-bonded organic framework with large-scale void regulation and adaptive guest accommodation abilities, *Nat. Commun.*, 2019, **10**, 3074.
12. C. G. Gruber, L. Frey, R. Guntermann, D. D. Medina and E. Cortés, Early stages of covalent organic framework formation imaged in operando, *Nature*, 2024, **630**, 872-877.
13. A. Puthukkudi, S. Nath, P. Shee, A. Dutta, C. V. Rajput, S. Bommakanti, J. Mohapatra, M. Samal, S. Anwar, S. Pal and B. P. Biswal, Terahertz Conductivity of Free-Standing 3D Covalent Organic Framework Membranes Fabricated via Triple-Layer-Dual Interfacial Approach, *Adv. Mater.*, 2024, **36**, 2312960.
14. J. Yang, S. Ghosh, J. Roeser, A. Acharjya, C. Penschke, Y. Tsutsui, J. Rabeah, T. Wang, S. Y. Djoko Tameu, M.-Y. Ye, J. Grüneberg, S. Li, C. Li, R. Schomäcker, R. Van De Krol, S. Seki, P. Saalfrank and A. Thomas, Constitutional isomerism of the linkages in donor–acceptor covalent organic frameworks and its impact on photocatalysis, *Nat. Commun.*, 2022, **13**, 6317.

View Article Online
DOI: 10.1039/D5SC04390E

15. Q. Wang, C. Wang, K. Zheng, B. Wang, Z. Wang, C. Zhang and X. Long, Positional Thiophene Isomerization: A Geometric Strategy for Precisely Regulating the Electronic State of Covalent Organic Frameworks to Boost Oxygen Reduction, *Angew. Chem. Int. Ed.*, 2024, **63**, e202320037.
16. P.-J. Tian, X.-H. Han, Q.-Y. Qi and X. Zhao, An Azulene-Based Crystalline Porous Covalent Organic Framework for Efficient Photothermal Conversion, *Small*, 2024, **20**, 2307635.
17. C.-Q. Han, J.-X. Guo, S. Sun, Z.-Y. Wang, L. Wang and X.-Y. Liu, Impact of Imine Bond Orientations and Acceptor Groups on Photocatalytic Hydrogen Generation of Donor–Acceptor Covalent Organic Frameworks, *Small*, 2024, **20**, 2405887.
18. J.-X. Fu, Y. Liu, L.-H. Chen, W.-K. Han, X. Liu, J.-X. Shao, X. Yan and Z.-G. Gu, Positional Isomers of Covalent Organic Frameworks for Indoor Humidity Regulation, *Small*, 2023, **19**, 2303897.
19. T. Wang, M. Li, Y. Chen, X. Che, F. Bi, Y. Yang, R. Yang and C. Li, Regioisomeric Benzotriazole-Based Covalent Organic Frameworks for High Photocatalytic Activity, *ACS Catal.*, 2023, **13**, 15439-15447.
20. Y. Guo, S. Li and M. Shao, Two-Dimensional Covalent Organic Framework Isomers Induce Different Properties, *ACS Appl. Electron. Mater.*, 2024, **6**, 214-220.
21. H. Chen, D. Li, M. Lin, Q. Wang, Y. Zou, J. Ran, Y. Xing and X. Long, Regulating the Isomerization Geometry and Energy State of Covalent Organic Frameworks for Enhanced Oxygen Reduction Activity, *Adv. Mater.*, 2025, **37**, 2500063.
22. W. Song, S. Chen, X. Ren, X. Su, C. Song, Y. Li, L. Chen and F. Bai, Isomeric Covalent Organic Frameworks for High-Efficiency Photocatalytic CO2 Reduction: Substituent Position Effect, *Small*, 2025, **21**, 2409117.
23. B. Feng, X. Chen, P. Yan, S. Huang, C. Lu, H. Ji, J. Zhu, Z. Yang, K. Cao and X. Zhuang, Isomeric Dual-Pore Two-Dimensional Covalent Organic Frameworks, *J. Am. Chem. Soc.*, 2023, **145**, 26871-26882.
24. W. Zhang, M. Sun, J. Cheng, X. Wu and H. Xu, Regulating Electron Distribution in Regioisomeric Covalent Organic Frameworks for Efficient Solar-Driven Hydrogen Peroxide Production, *Adv. Mater.*, 2025, **37**, 2500913.
25. T. P. Kaloni, P. K. Giesbrecht, G. Schreckenbach and M. S. Freund, Polythiophene: From Fundamental Perspectives to Applications, *Chem. Mater.*, 2017, **29**, 10248-10283.
26. M. E. Cinar and T. Ozturk, Thienothiophenes, Dithienothiophenes, and Thienoacenes: Syntheses, Oligomers, Polymers, and Properties, *Chem. Rev.*, 2015, **115**, 3036-3140.
27. G. H. V. Bertrand, V. K. Michaelis, T.-C. Ong, R. G. Griffin and M. Dincă, Thiophene-based covalent organic frameworks, *Proc. Natl. Acad. Sci.*, 2013, **110**, 4923.
28. R. Caballero, B. Cohen and M. Gutiérrez, Thiophene-Based Covalent Organic Frameworks: Synthesis, Photophysics and Light-Driven Applications, *Molecules*, 2021, **26**, 7666-7686.
29. S. Wang, L. Da, J. Hao, J. Li, M. Wang, Y. Huang, Z. Li, Z. Liu and D. Cao, A Fully Conjugated 3D Covalent Organic Framework Exhibiting Band-like Transport with Ultrahigh Electron Mobility, *Angew. Chem. Int. Ed.*, 2021, **60**, 9321-9325.
30. S. Wang, X.-X. Li, L. Da, Y. Wang, Z. Xiang, W. Wang, Y.-B. Zhang and D. Cao, A Three-Dimensional sp2 Carbon-Conjugated Covalent Organic Framework, *J. Am. Chem. Soc.*, 2021, **143**, 15562-15566.
31. Y. Wang, Z. Qiao, H. Li, R. Zhang, Z. Xiang, D. Cao and S. Wang, Molecular Engineering for Modulating Photocatalytic Hydrogen Evolution of Fully Conjugated 3D Covalent Organic Frameworks, *Angew. Chem. Int. Ed.*, 2024, **63**, e202404726.
32. X. Zheng, W. Qiu, J. Cui, H. Liu, Y. Zhao, J. Zhang, Z. Zhang and Y. Zhao, Donor-Acceptor Interactions Enhanced Colorimetric Sensors for Both Acid and Base Vapor Based on Two-Dimensional Covalent Organic Frameworks, *Chem. Eur. J.*, 2024, **30**, e202303004.
33. S. Hou, G. Liu, H. Gao, H. Li and X. Liang, Highly Efficient Aggregation-induced Electrochemiluminescence Performance of Covalent Organic Frameworks with Electron-rich Conjugated Structures, *Chem. Eur. J.*, 2025, **31**, e202403820.

View Article Online
DOI: 10.1039/D5SC04390E

34. Y. Liu, H. Zhang, H. Yu, Z. Liao, S. Paasch, S. Xu, R. Zhao, E. Brunner, M. Bonn, H. I. Wang, T. Heine, M. Wang, Y. Mai and X. Feng, A Thiophene Backbone Enables Two-Dimensional Poly(arylene vinylene)s with High Charge Carrier Mobility, *Angew. Chem. Int. Ed.*, 2023, **62**, e202305978.
35. R. Bao, Z. Xiang, Z. Qiao, Y. Yang, Y. Zhang, D. Cao and S. Wang, Designing Thiophene-Enriched Fully Conjugated 3D Covalent Organic Framework as Metal-Free Oxygen Reduction Catalyst for Hydrogen Fuel Cells, *Angew. Chem. Int. Ed.*, 2023, **62**, e202216751.
36. Z.-M. Yang, Y. Wang, M.-H. Zhang, Z.-Y. Hou, S.-P. Zhao, X. Han, S. Yuan, J. Su, Z. Jin and J.-L. Zuo, Electroactive tetrathiafulvalene-based covalent organic framework with thiophene units as anode for high-performance hybrid lithium-ion capacitors: Dedicated to Professor Hong-Cai Zhou on the occasion of his 60th birthday, *Energy Storage Mater.*, 2025, **75**, 104038.
37. H. Wei, J. Ning, X. Cao, X. Li and L. Hao, Benzotrithiophene-Based Covalent Organic Frameworks: Construction and Structure Transformation under Ionothermal Condition, *J. Am. Chem. Soc.*, 2018, **140**, 11618-11622.
38. N. Keller, D. Bessinger, S. Reuter, M. Calik, L. Ascherl, F. C. Hanusch, F. Auras and T. Bein, Oligothiophene-Bridged Conjugated Covalent Organic Frameworks, *J. Am. Chem. Soc.*, 2017, **139**, 8194-8199.
39. T. Sick, J. M. Rotter, S. Reuter, S. Kandambeth, N. N. Bach, M. Döblinger, J. Merz, T. Clark, T. B. Marder, T. Bein and D. D. Medina, Switching on and off Interlayer Correlations and Porosity in 2D Covalent Organic Frameworks, *J. Am. Chem. Soc.*, 2019, **141**, 12570-12581.
40. W. Wang, D. Huang, W. Zheng, X. Zhao, K. He, H. Pang and Y. Xiang, Construction of Amide-Linked Covalent Organic Frameworks by N-Heterocyclic Carbene-Mediated Selective Oxidation for Photocatalytic Dehalogenation, *Chem. Mater.*, 2023, **35**, 7154-7163.
41. J. I. Feldblyum, C. H. McCreery, S. C. Andrews, T. Kurosawa, E. J. G. Santos, V. Duong, L. Fang, A. L. Ayzner and Z. Bao, Few-layer, large-area, 2D covalent organic framework semiconductor thin films, *Chem. Commun.*, 2015, **51**, 13894-13897.
42. B. Cui, X. Zheng, J. Wang, D. Liu, S. Xie and B. Huang, Realization of Lieb lattice in covalent-organic frameworks with tunable topology and magnetism, *Nat. Commun.*, 2020, **11**, 66.
43. A. L. Sharpe, E. J. Fox, A. W. Barnard, J. Finney, K. Watanabe, T. Taniguchi, M. A. Kastner and D. Goldhaber-Gordon, Emergent ferromagnetism near three-quarters filling in twisted bilayer graphene, *Science*, 2019, **365**, 605-608.
44. E. Jin, M. Asada, Q. Xu, S. Dalapati, M. A. Addicoat, M. A. Brady, H. Xu, T. Nakamura, T. Heine, Q. Chen and D. Jiang, Two-dimensional sp2 carbon–conjugated covalent organic frameworks, *Science*, 2017, **357**, 673-676.
45. D. Blätte, F. Ortmann and T. Bein, Photons, Excitons, and Electrons in Covalent Organic Frameworks, *J. Am. Chem. Soc.*, 2024, **146**, 32161-32205.
46. S. Chen, H. Wang, Z. Ou, H. Liu, J. Zhou, P. Hu, Y. Wang, D. Zhong and H. Ji, On-Surface Synthesis of 2D Porphyrin-Based Covalent Organic Frameworks Using Terminal Alkynes, *Chem. Mater.*, 2021, **33**, 8677-8684.
47. T. Friščić, C. Mottillo and H. M. Titi, Mechanochemistry for Synthesis, *Angew. Chem. Int. Ed.*, 2020, **59**, 1018-1029.
48. B. P. Biswal, S. Chandra, S. Kandambeth, B. Lukose, T. Heine and R. Banerjee, Mechanochemical Synthesis of Chemically Stable Isoreticular Covalent Organic Frameworks, *J. Am. Chem. Soc.*, 2013, **135**, 5328-5331.
49. J. Hu, Z. Huang and Y. Liu, Beyond Solvothermal: Alternative Synthetic Methods for Covalent Organic Frameworks, *Angew. Chem. Int. Ed.*, 2023, **62**, e202306999.
50. S. T. Emmerling, L. S. Germann, P. A. Julien, I. Moudrakovski, M. Etter, T. Friščić, R. E. Dinnebier and B. V. Lotsch, In situ monitoring of mechanochemical covalent organic framework formation reveals templating effect of liquid additive, *Chem*, 2021, **7**, 1639-1652.

View Article Online
DOI: 10.1039/D5SC04390E

51. G. Das, D. Balaji Shinde, S. Kandambeth, B. P. Biswal and R. Banerjee, Mechanosynthesis of imine, β-ketoenamine, and hydrogen-bonded imine-linked covalent organic frameworks using liquid-assisted grinding, *Chem. Commun.*, 2014, **50**, 12615-12618.
52. S. Karak, S. Kandambeth, B. P. Biswal, H. S. Sasmal, S. Kumar, P. Pachfule and R. Banerjee, Constructing Ultraporous Covalent Organic Frameworks in Seconds via an Organic Terracotta Process, *J. Am. Chem. Soc.*, 2017, **139**, 1856-1862.
53. E. Hamzehpoor, F. Effaty, T. H. Borchers, R. S. Stein, A. Wahrhaftig-Lewis, X. Ottenwaelder, T. Friščić and D. F. Perepichka, Mechanochemical Synthesis of Boroxine-linked Covalent Organic Frameworks, *Angew. Chem. Int. Ed.*, 2024, **63**, e202404539.
54. D. B. Shinde, H. B. Aiyappa, M. Bhadra, B. P. Biswal, P. Wadge, S. Kandambeth, B. Garai, T. Kundu, S. Kurungot and R. Banerjee, A mechanochemically synthesized covalent organic framework as a proton-conducting solid electrolyte, *J. Mater. Chem. A*, 2016, **4**, 2682-2690.
55. Y. Peng, G. Xu, Z. Hu, Y. Cheng, C. Chi, D. Yuan, H. Cheng and D. Zhao, Mechanoassisted Synthesis of Sulfonated Covalent Organic Frameworks with High Intrinsic Proton Conductivity, *ACS Appl. Mater. Interfaces*, 2016, **8**, 18505-18512.
56. A. Jati, A. K. Mahato, D. Chanda, P. Kumar, R. Banerjee and B. Maji, Photocatalytic Decarboxylative Fluorination by Quinone-Based Isoreticular Covalent Organic Frameworks, *J. Am. Chem. Soc.*, 2024, **146**, 23923-23932.
57. Y. Yang, W. Zhao, H. Niu and Y. Cai, Mechanochemical Construction 2D/2D Covalent Organic Nanosheets Heterojunctions Based on Substoichiometric Covalent Organic Frameworks, *ACS Appl. Mater. Interfaces*, 2021, **13**, 42035-42043.
58. N. Brown, Z. Alsudairy, R. Behera, F. Akram, K. Chen, K. Smith-Petty, B. Motley, S. Williams, W. Huang, C. Ingram and X. Li, Green mechanochemical synthesis of imine-linked covalent organic frameworks for high iodine capture, *Green Chem.*, 2023, **25**, 6287-6296.
59. H. Chen, D. Feng, F. Wei, F. Guo and A. K. Cheetham, Hydrogen-Bond-Regulated Mechanochemical Synthesis of Covalent Organic Frameworks: Cocrystal Precursor Strategy for Confined Assembly, *Angew. Chem. Int. Ed.*, 2024, **64**, e202415454.
60. N. Brown, Q. Zhang, Z. Alsudairy, C. Dun, Y. Nailwal, A. Campbell, C. Harrod, L. Chen, S. Williams, J. J. Urban, Y. Liu and X. Li, Mechanochemical in Situ Encapsulation of Palladium in Covalent Organic Frameworks, *ACS Sustainable Chem. Eng.*, 2024, **12**, 13535-13543.
61. Y. Hu, W.-K. Han, Y. Liu, R.-M. Zhu, X. Yan, H. Pang and Z.-G. Gu, Mechanochemical Transition from a Hydrogen-Bonded Organic Framework to Covalent Organic Frameworks, *ACS Materials Lett.*, 2023, **5**, 2534-2541.
62. Y. Nailwal, Q. Zhang, N. Brown, Z. Alsudairy, C. Harrod, M. H. Uddin, F. Akram, J. Li, Y. Liu and X. Li, A Rapid, Sustainable, One-step Mechanochemical Strategy for Synthesizing Gold Nanoparticle-Doped Covalent Organic Frameworks, *Chem. Eur. J.*, 2025, **31**, e202500339.
63. K. Asokan, M. K. Patil, S. P. Mukherjee, S. B. Sukumaran and T. Nandakumar, Scalable Mechanochemical Synthesis of β-Ketoenamine-linked Covalent Organic Frameworks for Methane Storage, *Chem. Asian J.*, 2022, **17**, e202201012.
64. S. Hutsch, A. Leonard, S. Grätz, M. V. Höfler, T. Gutmann and L. Borchardt, Mechanochemical Cyclotrimerization: A Versatile Tool to Covalent Organic Frameworks with Tunable Stacking Mode, *Angew. Chem. Int. Ed.*, 2024, **63**, e202403649.
65. J. M. Marrett, F. Effaty, X. Ottenwaelder and T. Friščić, Mechanochemistry for Metal–Organic Frameworks and Covalent–Organic Frameworks (MOFs, COFs): Methods, Materials, and Mechanisms, *Adv. Mater.*, 2025, DOI: 10.1002/adma.202418707, 2418707.
66. Y. Nailwal, B. Baker, Z. Alsudairy, M. El Hariri El Nokab, Q. Zhang, T. Wang, S. Cai, Y. Liu and X. Li, Ambient mechanosynthesis of flexible two-dimensional covalent organic frameworks, *Green Chem.*, 2025, **27**, 8848-8857.
67. C. Zou, Q. Li, Y. Hua, B. Zhou, J. Duan and W. Jin, Mechanical Synthesis of COF Nanosheet Cluster and Its Mixed Matrix Membrane for Efficient CO2 Removal, *ACS Appl. Mater. Interfaces*, 2017, **9**, 29093-29100.

View Article Online
DOI: 10.1039/D5SC04390E

68. J.-J. Liu, J. Yang, J.-L. Wang, Z.-F. Chang, B. Li, W.-T. Song, Z. Zhao, X. Lou, J. Dai and F. Xia, Tetrathienylethene based red aggregation-enhanced emission probes: super red-shifted mechanochromic behavior and highly photostable cell membrane imaging, *Mater. Chem. Front.*, 2018, **2**, 1126-1136.
69. L. Liu, B. Yang, T. J. Katz and M. K. Poindexter, Improved methodology for photocyclization reactions, *J. Org. Chem.*, 1991, **56**, 3769-3775.
70. L. Viglianti, N. L. C. Leung, N. Xie, X. Gu, H. H. Y. Sung, Q. Miao, I. D. Williams, E. Licandro and B. Z. Tang, Aggregation-induced emission: mechanistic study of the clusteroluminescence of tetrathienylethene, *Chem. Sci.*, 2017, **8**, 2629-2639.
71. A. Yamamoto, E. Ohta, N. Kishigami, N. Tsukahara, Y. Tomiyori, H. Sato, Y. Matsui, Y. Kano, K. Mizuno and H. Ikeda, Synthesis and basic properties of tetrathieno[2,3-a:3′,2′-c:2″,3″-f:3‴,2‴-h]naphthalene: a new π-conjugated system obtained by photoinduced electrocyclization–dehydrogenation reactions of tetra(3-thienyl)ethene, *Tetrahedron Lett.*, 2013, **54**, 4049-4053.
72. T. Friščić, S. L. Childs, S. A. A. Rizvi and W. Jones, The role of solvent in mechanochemical and sonochemical cocrystal formation: a solubility-based approach for predicting cocrystallisation outcome, *CrystEngComm*, 2009, **11**, 418-426.
73. A. Yamamoto, Y. Matsui, T. Asada, M. Kumeda, K. Takagi, Y. Suenaga, K. Nagae, E. Ohta, H. Sato, S. Koseki, H. Naito and H. Ikeda, Amorphous Solid Simulation and Trial Fabrication of the Organic Field-Effect Transistor of Tetrathienonaphthalenes Prepared by Using Microflow Photochemical Reactions: A Theoretical Calculation-Inspired Investigation, *J. Org. Chem.*, 2016, **81**, 3168-3176.
74. M. R. Rao, Y. Fang, S. De Feyter and D. F. Perepichka, Conjugated Covalent Organic Frameworks via Michael Addition–Elimination, *J. Am. Chem. Soc.*, 2017, **139**, 2421-2427.
75. L. Cusin, H. Peng, A. Ciesielski and P. Samorì, Chemical Conversion and Locking of the Imine Linkage: Enhancing the Functionality of Covalent Organic Frameworks, *Angew. Chem. Int. Ed.*, 2021, **60**, 14236-14250.
76. J. L. Segura, S. Royuela and M. Mar Ramos, Post-synthetic modification of covalent organic frameworks, *Chem. Soc. Rev.*, 2019, **48**, 3903-3945.
77. F. Haase, E. Troschke, G. Savasci, T. Banerjee, V. Duppel, S. Dörfler, M. M. J. Grundei, A. M. Burow, C. Ochsenfeld, S. Kaskel and B. V. Lotsch, Topochemical conversion of an imine- into a thiazole-linked covalent organic framework enabling real structure analysis, *Nat. Commun.*, 2018, **9**, 2600.
78. Y. Yang, L. Yu, T. Chu, H. Niu, J. Wang and Y. Cai, Constructing chemical stable 4-carboxyl-quinoline linked covalent organic frameworks via Doebner reaction for nanofiltration, *Nat. Commun.*, 2022, **13**, 2615.
79. P. Das, G. Chakraborty, J. Roeser, S. Vogl, J. Rabeah and A. Thomas, Integrating Bifunctionality and Chemical Stability in Covalent Organic Frameworks via One-Pot Multicomponent Reactions for Solar-Driven H2O2 Production, *J. Am. Chem. Soc.*, 2023, **145**, 2975-2984.
80. E. Jin, K. Geng, K. H. Lee, W. Jiang, J. Li, Q. Jiang, S. Irle and D. Jiang, Topology-Templated Synthesis of Crystalline Porous Covalent Organic Frameworks, *Angew. Chem. Int. Ed.*, 2020, **59**, 12162-12169.
81. D. B. Patel, D. P. Rajani, S. D. Rajani and H. D. Patel, A green synthesis of quinoline-4-carboxylic derivatives using p-toluenesulfonic acid as an efficient organocatalyst under microwave irradiation and their docking, molecular dynamics, ADME-Tox and biological evaluation, *J. Heterocyclic Chem.*, 2020, **57**, 1524-1544.
82. G. C. Muscia, J. P. Carnevale, M. Bollini and S. E. Asís, Microwave-assisted döbner synthesis of 2-phenylquinoline-4-carboxylic acids and their antiparasitic activities, *J. Heterocyclic Chem.*, 2008, **45**, 611-614.
83. R. Gutzler and D. F. Perepichka, π-Electron Conjugation in Two Dimensions, *J. Am. Chem. Soc.*, 2013, **135**, 16585-16594.

View Article Online
DOI: 10.1039/D5SC04390E

84. E. Hamzehpoor, P. Ghamari, Y. Tao, M. G. Rafique, Z. Zhang, M. Salehi, R. S. Stein, J. Ramos-Sanchez, A. W. Laramée, G. Cosa, C. Pellerin, A. Seifitokaldani, R. Z. Khaliullin and D. F. Perepichka, Azatriangulene-Based Conductive C═C Linked Covalent Organic Frameworks with Near-Infrared Emission, *Adv. Mater.*, 2024, **36**, 2413629.
85. S. Chandra, T. Kundu, S. Kandambeth, R. BabaRao, Y. Marathe, S. M. Kunjir and R. Banerjee, Phosphoric Acid Loaded Azo (−N═N−) Based Covalent Organic Framework for Proton Conduction, *J. Am. Chem. Soc.*, 2014, **136**, 6570-6573.
86. X. Meng, H.-N. Wang, S.-Y. Song and H.-J. Zhang, Proton-conducting crystalline porous materials, *Chem. Soc. Rev.*, 2017, **46**, 464-480.
87. T. Jadhav, Y. Fang, C.-H. Liu, A. Dadvand, E. Hamzehpoor, W. Patterson, A. Jonderian, R. S. Stein and D. F. Perepichka, Transformation between 2D and 3D Covalent Organic Frameworks via Reversible [2 + 2] Cycloaddition, *J. Am. Chem. Soc.*, 2020, **142**, 8862-8870.
88. Y. Yang, X. He, P. Zhang, Y. H. Andaloussi, H. Zhang, Z. Jiang, Y. Chen, S. Ma, P. Cheng and Z. Zhang, Combined Intrinsic and Extrinsic Proton Conduction in Robust Covalent Organic Frameworks for Hydrogen Fuel Cell Applications, *Angew. Chem. Int. Ed.*, 2020, **59**, 3678-3684.

View Article Online
DOI: 10.1039/D5SC04390E

The data that support the findings of this study are available in the supplementary material of this article.